



Intercomparison of global reanalysis precipitation for flood risk modelling

Fergus McClean¹, Richard Dawson¹, and Chris Kilsby^{1,2}

¹School of Engineering, Newcastle University, Newcastle upon Tyne, NE1 7RU, UK

²Willis Research Network, 51 Lime St., London, EC3M 7DQ, UK

1 Corresponding author: Fergus McClean <fergus.mcclean@newcastle.ac.uk>

2 Abstract

3 Reanalysis datasets are increasingly used to drive flood models, especially for continental and global
4 analysis, and in areas of data scarcity. However, the consequence of this for risk estimation has not been
5 fully explored. We investigate the impact of using four reanalysis products (ERA-5, CFSR, MERRA-2
6 and JRA-55) on simulations of historic flood events in Northern England. These results are compared to
7 a benchmark national gauge-based product (CEH-GEAR1hr). All reanalysis products predicted fewer
8 buildings would be inundated by the events than the national dataset. JRA-55 was the worst by a
9 significant margin, underestimating by 40% compared with 14-18% for the other reanalysis products.
10 CFSR estimated building inundation the most accurately, while ERA-5 demonstrated the lowest error
11 in terms of river stage (29.4%) and floodplain depth (28.6%). Accuracy varied geographically and
12 no product performed the best across all basins. Global reanalysis products provide a useful resource
13 for flood modelling where no other data is available, but they should be used with caution. Until a
14 more systematic international strategy for the collection of rainfall data ensures more complete global
15 coverage of validation data, multiple reanalysis products should be used concurrently to capture the
16 range of uncertainties.

17 Introduction

18 The primary drivers of pluvial and fluvial flooding are precipitation events. The duration, intensity and
19 spatial extent of these events can all affect the depth and extent of any flooding caused. Therefore, the
20 choice of precipitation data when simulating floods is critical. Inaccurate precipitation will undoubtedly
21 lead to a spurious and potentially misleading understanding of the risk posed by a given event. This
22 effect is further exacerbated when low-quality precipitation data is used to project risk into the future,
23 with planning decisions being made based on the results. Unfortunately, understanding which source of
24 precipitation is most appropriate is challenging. There is also spatial variation in the availability and
25 quality of precipitation data. High-quality data is often collected by national or regional authorities but
26 can be inaccessible or difficult to obtain, therefore continental or global precipitation datasets, such as
27 reanalysis products, are a popular option despite their generally lower resolution and accuracy.

28 Reanalysis precipitation data has been widely used in large-scale flood risk modelling (Alfieri et al., 2013;
29 Andreadis et al., 2017; Pappenberger, Dutra, Wetterhall, & Cloke, 2012; Schumann et al., 2013; Seyyedi,
30 Anagnostou, Beighley, & McCollum, 2015; Winsemius, Beek, Jongman, Ward, & Bouwman, 2013; Xu,
31 Xu, Chen, & Chen, 2016). The main advantages of reanalysis products are their vast spatiotemporal
32 coverage and ease of access. In areas with a limited number of rain gauges that can provide high-
33 quality observations, reanalysis products are often the best or only source of precipitation inputs for



34 flood simulations. However, there is no guarantee that they are able to accurately represent extreme
35 events and subsequently characterise flood risk. As a range of reanalysis datasets are available, there is
36 also the question of which is more suitable for the application.

37 The influence of reanalysis data on flood risk estimates has previously been explored in part. Sampson
38 et al. (2014) found that the loss ratio decreased by 8.5 times when using a reanalysis product (ERA-
39 Interim) instead of a satellite rainfall product (CMORPH) in their catastrophe risk model of Dublin.
40 Andreadis et al. (2017) compared flood models driven using an ensemble of parameters from 20CRv2 to
41 a benchmark using observed flow boundary conditions and found that, overall, 20CRv2 only captured
42 15.7% of the benchmark inundated area. Mahto and Mishra (2019) used ERA-5, ERA-Interim, CFSR,
43 JRA-55 and MERRA-2 to drive VIC and simulate monsoon season runoff in India. CFSR and JRA-
44 55 resulted in a strong positive bias, compared to a national precipitation dataset, while MERRA-2
45 strongly underestimated runoff. The two ERA products showed a much less prominent positive bias.
46 While their study represents one of the first intercomparisons of different reanalysis precipitation products
47 for runoff modelling, it does not go as far as looking at the consequences for flood impacts. Meanwhile,
48 Chawla and Mujumdar (2020) demonstrate a strong negative bias in flood discharge when using CFSR
49 in the Himalayas. This is indicative of the spatial variability in accuracy inherent in reanalysis datasets,
50 driven largely by assimilation data availability. Winsemius et al. (2013) compared flood impacts from
51 the GLOFRIS model cascade, which uses ERA-Interim, with The OFDA/CRED International Disaster
52 Database (EM-DAT). However, the effect of using a different source of precipitation was not assessed
53 and therefore the impact of using reanalysis data on the cascade is unknown.

54 This paper extends previous studies by undertaking a systematic intercomparison of how modern re-
55 analysis products compare when used to drive a hydrodynamic flood model. This provides important
56 insights to inform the selection of data for flood modelling in data-sparse regions as well as a more general
57 assessment of how well extreme rainfall events are captured in each product. To provide further context
58 and identify the potential effects on flood risk assessments, the flood model outputs are subsequently
59 used to estimate the number of buildings that would be inundated by each rainfall product.

60 Methodology

61 Study Area

62 To assess the performance of global reanalysis precipitation, more reliable gauge-based data is required
63 as a baseline to validate against. However, the quantity and quality of gauge observations are limited
64 across much of the globe, particularly in sparsely populated and poorer regions. Local gauge data may
65 in fact be of lower accuracy than the large scale products if the rain gauges on the ground are of poor
66 quality or have been influenced by human error. There is no way to check which is more correct by
67 looking at precipitation alone and an independent source of data is required. River flow data has been
68 used for this purpose in the past Beck et al. (2017) and presents a viable option for assessing precipitation
69 performance in the context of flood events. To fulfil the requirements of high-quality local precipitation
70 and river flow observations, an area of northern England, encompassing the Tyne, Tees, Eden, Wear
71 and Lune basins (Figure 1) was selected for this study. The relatively simple flood response of these
72 steep, surface water dominated basins, and the occurrence of recent flood events, means they provide a
73 suitable testbed for investigating the effects of using global reanalysis products for more localised flood
74 risk modelling.

75

76 Model Setup

77 The City Catchment Analysis Tool (CityCAT) (Glenis, Kutija, & Kilsby, 2018), a hydrodynamic surface
78 water flood model, was used to simulate flooding in this study. CityCAT represents spatial rainfall
79 fields falling directly onto uniformly gridded elevation surfaces and propagating according to the shallow
80 water equations. The system is suitable for this study as it is able to directly capture the effects of
81 rainfall on flood depths without requiring any intermediate steps. Model domains within the study area

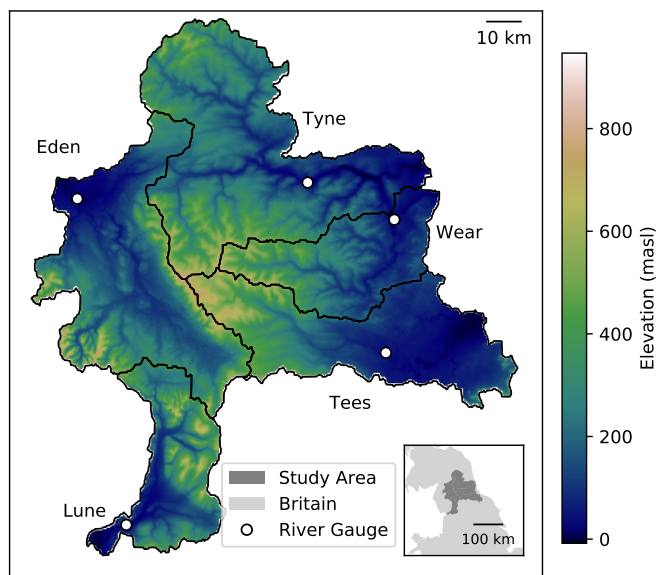


Figure 1: The location and topography of basins within the study area, illustrated using OS Terrain 50.

82 were delineated using HydroBASINS (Lehner & Grill, 2014). Water depths were output every hour for
83 each grid cell within the domain and then extracted at each gauge location (Figure 1). The Manning's
84 coefficient for all domains was uniformly defined as 0.03 (Chow, 1959) and the land surface was assumed
85 to be impermeable given the extreme nature of the selected events (described below). As this study
86 primarily aims to compare model results with one another, the absolute accuracy of the hydrodynamic
87 model is not the focus and therefore the friction and infiltration configurations are not critical.

88 Rainfall

89 Four global reanalysis products (JRA-55, MERRA-2, ERA-5 and CFSR) have been selected and compared
90 against CEH-GEAR1hr, used here as a benchmark. Each rainfall dataset is described below and
91 key characteristics are shown in Table 1. The reanalysis products were selected based on their high
92 spatiotemporal resolution, open availability and suitable duration. Events between the start and end
93 dates of CEH-GEAR1hr (1990-2014) were selected based on the peak stage at the most downstream
94 river gauge within each basin (Table 2). This identified the most extreme rainfall events, independently
95 of the rainfall data itself. Different events were selected for each basin as the largest extremes may have
96 occurred at different times in different areas. Each identified event was only simulated in the basin in
97 which it was observed, to enable river gauge records to be used for validation. Simulations were
98 commenced two weeks before the discharge peaks and ran until one week after. This was to allow model
99 spinup and characterisation of hydrograph recession. The sensitivity to run duration was not explicitly
100 assessed here but the duration was sufficient in all cases to ensure adequate accounting for antecedent
101 rainfall and return to normal flow conditions. The events, according to each dataset, are mapped in
102 Figure 2. CEH-GEAR1hr contained, on average, higher rainfall totals than the reanalysis products and
103 JRA-55 represented only approximately half as much precipitation as other reanalysis products. Each
104 rainfall value was converted into a rate ($\text{kg m}^{-2} \text{s}^{-1}$) at the observed times and each point on the grid
105 was converted into an area with a width and height equivalent to the horizontal and vertical resolution
106 of the dataset. These areas were then re-projected into British National Grid as cartesian coordinates



Dataset	DOI	Resolution	Coverage	Period	Frequency
CEH-GEAR1hr	10.5285/d4ddc781-25f3-423a-bba0-747cc82dc6fa	1 km	Great Britain	1990-2014	Hourly
ERA-5	10.24381/cds.adbb2d47	~30 km	Global	1979-	Hourly
MERRA-2	10.5067/7MCPBJ41Y0K6	~55 km	Global	1980-	Hourly
CFSR	10.5065/D6513W89	~35 km	Global	1979-2011	Hourly
JRA-55	10.5065/D6HH6H41	~60 km	Global	1958-	3 Hourly

Table 1: Precipitation products included in this study. Where the end of the period is not given, the product continues to be updated to the present day at the time of writing.

are required by CityCAT.

Basin	Stage Peak (m)	Peak Time	Start Time	End Time
Wear	4.1	2009-07-18 11:00:00	2009-07-04 11:00:00	2009-07-25 11:00:00
Tyne	6.3	2005-01-08 08:00:00	2004-12-25 08:00:00	2005-01-15 08:00:00
Tees	3.3	1995-01-31 20:15:00	1995-01-17 20:15:00	1995-02-07 20:15:00
Lune	7.1	1995-01-31 21:15:00	1995-01-17 21:15:00	1995-02-07 21:15:00
Eden	7.2	2005-01-08 14:30:00	2004-12-25 14:30:00	2005-01-15 14:30:00

Table 2: Event start and end times for each basin based on the observed stage peak at the most downstream gauge. Start times are two weeks before, and end times two weeks after, the observed stage peak times to allow for model spin-up and inclusion of hydrograph recession.

107

108 The Centre for Ecology and Hydrology provide an hourly version of their Gridded Estimates of Areal
109 Rainfall dataset (CEH-GEAR1hr) (Lewis et al., 2019). This hourly product is based on a daily product
110 which interpolates data from rain gauges using natural neighbour interpolation (Tanguy, 2019).
111 CEH-GEAR1hr uses nearest neighbour interpolation to maintain more realistic weather patterns and
112 unmoderated peak values. To ensure consistency between the hourly and daily versions, the daily totals
113 were maintained in the hourly dataset by scaling the interpolated values accordingly (Lewis et al., 2018).
114 This gauge-based dataset was used as a baseline to compare against the reanalysis products identified
115 below.

116 Japanese Meteorological Agency reanalysis 55 (JRA-55) replaces JRA-25, incorporating higher resolution
117 and better data assimilation, among other improvements (Japan Meteorological Agency, 2013; Kobayashi
118 et al., 2015). Suzuki et al. (2017) were able to effectively simulate continental river discharge using JRA-
119 55, however, they found large biases attributable to precipitation error in some regions.

120 Modern-Era Retrospective Analysis for Research and Applications 2 (MERRA-2) (Global Modeling and
121 Assimilation Office, 2015) builds upon its predecessor, MERRA (Rienecker et al., 2011), with reduced
122 biases in aspects of the water cycle, among other improvements (Gelaro et al., 2017). MERRA-2 uses
123 observed precipitation products to correct the forecasts and provide better estimates (Reichle et al.,
124 2017). Hua, Zhou, Nicholson, Chen, and Qin (2019) found that MERRA-2 was better at representing
125 rainfall climatology over Central Equatorial Africa than ERA-Interim and JRA-55, among others.

126 The European Centre for Medium-Range Weather Forecasts Reanalysis 5 product (ERA-5) (ECMWF,
127 2018) replaces and improves on ERA-Interim (Dee et al., 2011), which stopped being produced in August
128 2019. It supports an increased spatial and temporal resolution, along with an updated modelling and
129 data assimilation system, which has resulted in better representation of convective rainfall (Mahto &
130 Mishra, 2019). The land surface component is being used to calculate river discharge for the Global
131 Flood Awareness System (Harrigan et al., 2020). Albergel et al. (2018) found that ERA-5 resulted in
132 better estimates of river discharge than ERA-Interim when used to drive a land surface model of the
133 US. It has also been shown to outperform a range of other reanalysis products as part of a hydrological
134 model applied in two Indian basins (Mahto & Mishra, 2019).

135 The NCEP Climate Forecast System Reanalysis (CFSR) (Saha et al., 2010) replaces the previous
136 NCEP/NCAR reanalysis (Kalnay et al., 1996) and uses a very similar analysis system to MERRA-2

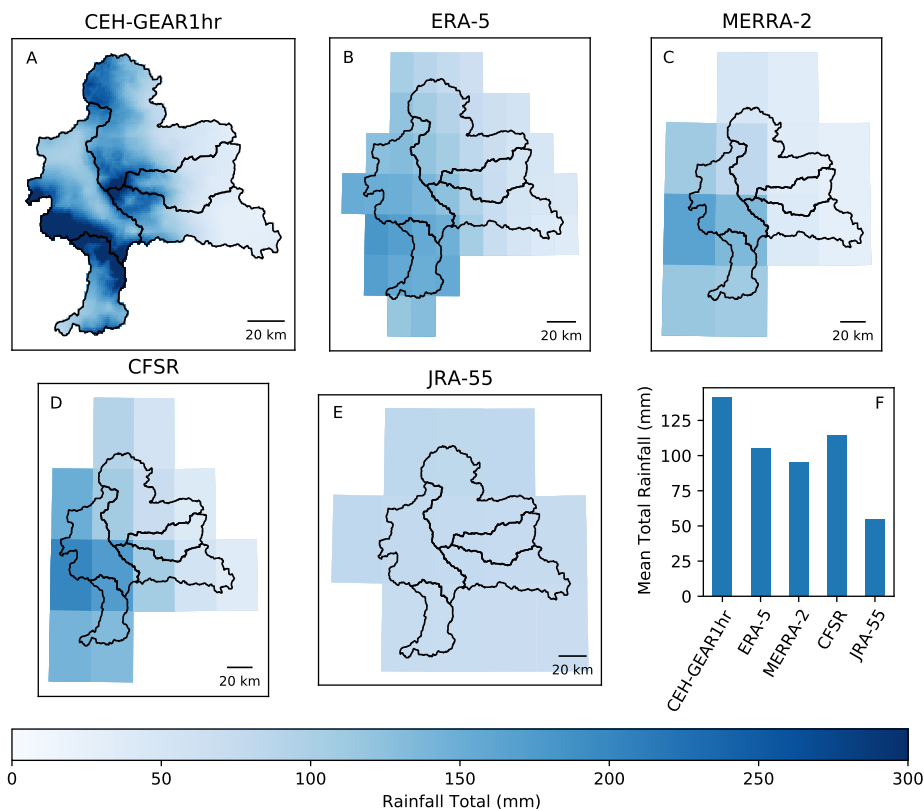


Figure 2: (A)-(E) show rainfall over the study area during the events in Table 2, according to each reanalysis dataset. (F) shows the total rainfall over the domain for all reanalysis datasets.

137 (Saha et al., 2010). Zhu, Xuan, Liu, and Xu (2016) demonstrated that CFSR was liable to overestimate
138 high streamflow in two Chinese basins using SWAT and highlighted that performance varied between
139 basins.

140

141 Digital Elevation Model

142 The terrain dataset used to represent the domain surface is a nationally and freely available Digital
143 Elevation Model (DEM) product from the Ordnance Survey, known as OS Terrain 50 (Ordnance Survey,
144 2017). This has been shown to perform best for flood risk modelling in a comparison with other DEMs
145 (McClellan, Dawson, & Kilsby, 2020). The product is based on airborne LIDAR and is corrected using
146 a combination of automated and manual processes to create a bare earth surface with raised structures
147 removed. The dataset was clipped to the area of each basin and used directly within the models (Figure
148 1).



149 Exposure

150 Building outlines from OS VectorMapLocal (VML) (Ordnance Survey, 2020) were used to estimate
151 numbers of buildings inundated by each model. VML only represents individual buildings with a floor
152 area over 20 m² and each polygon may represent multiple buildings. Therefore, not all buildings are
153 included in the inundation totals. This is acceptable for this analysis which compares the relative
154 magnitude of flooding, rather than the absolute totals. Buildings from VML were classified as flooded if
155 they intersected any model cell above a typical property threshold of 0.3 m (Environment Agency, 2019).

156 Results

157 The performance of each simulation was compared in terms of the magnitude and timing of the hydro-
158 graph peak, the flood depth, and the number of buildings inundated (Table 3). ERA-5 outperformed
159 other reanalysis datasets in terms of hydrograph peak error and floodplain depth, however, CFSR pro-
160 duced more similar inundation levels to CEH-GEAR1hr and demonstrated more accurate peak timing.
161 JRA-55 performed significantly worse than other reanalysis products across all of these aggregated mea-
162 sures. The variability of each metric will now be assessed in more detail, including spatial variations in
163 performance.

Rainfall Source	Mean Absolute Peak Error (%)	Mean Absolute Peak Time Error (hrs)	Mean Absolute Inundation Error (%)	Median Floodplain Depth Error (%)
CEH-GEAR1hr	29.4	1.0		
ERA-5	29.4	4.2	16.1	-28.6
MERRA-2	49.2	3.4	18.4	-44.4
JRA-55	70.9	162.6	39.6	-66.7
CFSR	38.0	3.4	14.4	-33.3

Table 3: Summary of performance statistics for each model. Building inundation and floodplain depth errors are relative to CEH-GEAR1hr, therefore the CEG-GEAR1hr model has no values for these measures.

164 The maximum water depths according to models using each of the rainfall datasets are shown in Figure 3.
165 Overall, the spatial distribution of floodwater is similar, as the same DEM is used in all models. There
166 are noticeably higher depths along main river channels in the CEH-GEAR1hr results. JRA-55 presents
167 less clearly visible channels than the other models, particularly in the Lune and Tees basins. The
168 maps also illustrate that the MERRA-2 model produced lower depths in the Tyne basin than other
169 reanalysis precipitation datasets. Across all basins, ERA-5 and CFSR produced similar distributions of
170 error relative to the CEH-GEAR1hr results. The inter-quartile range of errors in MERRA-2 is narrower
171 but the median error is slightly further below zero than ERA-5 and CFSR. JRA-55 water depths were
172 significantly further below the other reanalysis datasets.

173 Time series of water depths were extracted from the models at each gauge location and compared with
174 the observed values (Figure 4). In all basins, apart from the Wear, CEH-GEAR1hr was closest to
175 the observed peaks and predicted the highest maximum depth. In the Wear basin, where all models
176 overestimated river stage, CEH-GEAR1hr was actually the least accurate. However, the observed values
177 may be misleading here as flows go out of bank above 3 metres and so peaks are truncated. JRA-
178 55 consistently severely underestimated river stage and only captured peaks in the Eden and Tyne
179 basins. ERA-5 and CFSR display relatively similar performance across all basins. Meanwhile, MERRA-
180 2 underestimated the peaks in the Eden and Tyne. All reanalysis products strongly underestimated the
181 flood peak in the Lune basin.

182 The total numbers of inundated buildings for each model are shown in Figure 5. In four out of five basins,
183 using CEH-GEAR1hr resulted in the highest number of inundated buildings. ERA-5 inundated the most

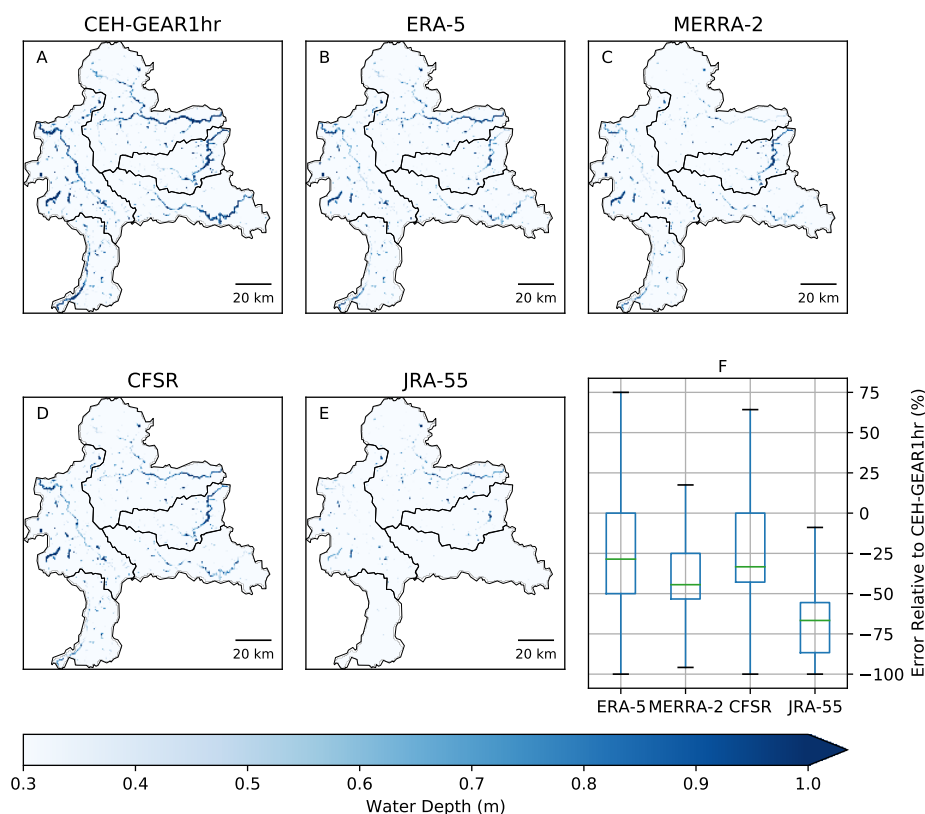


Figure 3: (A)-(E) show maximum water depth throughout the study area from models using each of the rainfall datasets. (F) shows the depth error of the reanalysis datasets relative to CEH-GEAR1hr across all cells, excluding outliers.

184 buildings in the Tees basin despite not being consistently higher than the other reanalysis datasets in
185 the other basins. JRA-55 inundated the lowest number of buildings by a large margin in all basins apart
186 from the Tyne, where it exceeded both MERRA-2 and CFSR. CFSR never resulted in either the highest
187 or lowest number of inundated buildings. There is general agreement between the rankings of modelled
188 peak water depth as shown in Figure 4 and the number of inundated buildings. Notable exceptions
189 include the Tees, where the high inundation levels predicted by ERA-5 were not replicated in its depth
190 peak, which was lower than CEH-GEAR1hr by a clear margin.

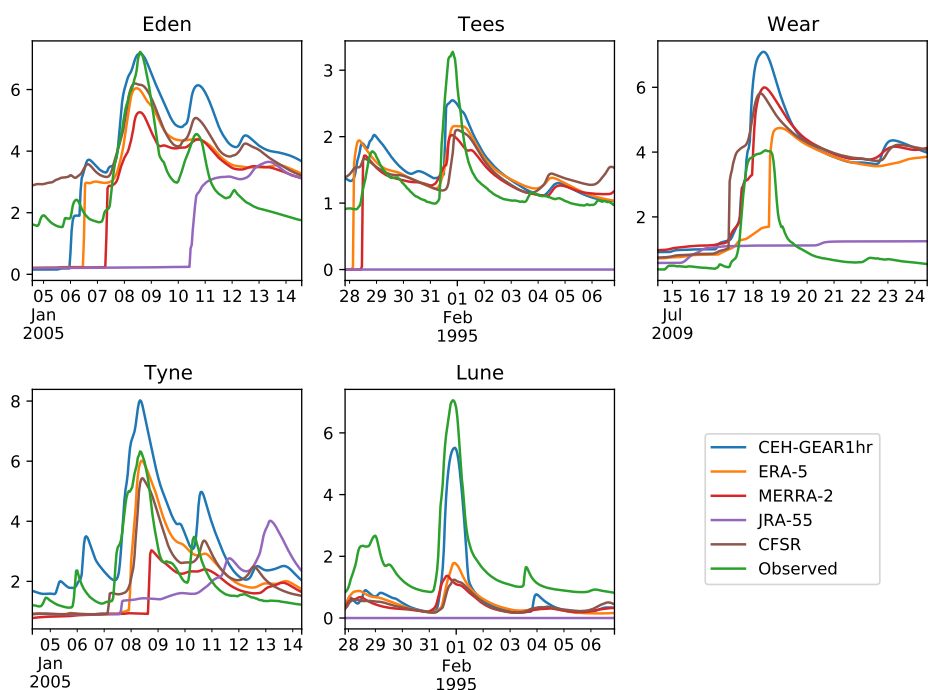


Figure 4: Stage hydrographs comparing water depths (m) from model results and observed values at each gauge.

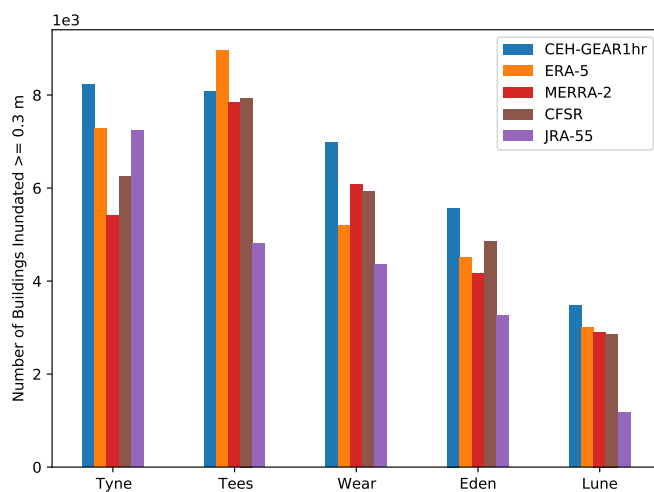


Figure 5: Number of buildings inundated above a threshold (0.3 m) per basin by each model.



191 Discussion

192 The results presented above demonstrate a persistent bias towards underestimation of flood depths and
193 impacts when using global reanalysis products in place of high-resolution gauge-based rainfall datasets.
194 The negative bias has been shown to exist in depths across the basins studied, at river gauging stations
195 and specifically at the locations of buildings, which correspond to built-up areas exposed to flooding. This
196 finding is in line with Sampson et al. (2014), who show ERA-Interim, an older product, underestimated
197 flood risk. Our results, however, do not indicate such a stark bias, perhaps because the products used
198 here are more modern and advanced than ERA-Interim. This is backed up by Towner et al. (2019) who
199 have demonstrated improved performance of ERA-5 over ERA-Interim using hydrological models of the
200 Amazon. Hirpa et al. (2016) also illustrate that ERA-Interim can underestimate flood risk, with spatial
201 variability, which further reinforces our finding. In contrast, Andreadis et al. (2017) find flood extent
202 to be overestimated (relative to a benchmark simulation) when using the 20CRv2 reanalysis product.
203 However, they did find that outflow discharge was underestimated, which agrees with our results. Their
204 assessment of flood extent did not include flood depths or effects on the inundation of exposed assets,
205 as we have done here, which may explain the observed overestimation to some degree. We also did not
206 replicate the underestimation of streamflow found by Zhu et al. (2016) when using CFSR. Though, it is
207 difficult to draw direct comparisons given the major differences in methodology between studies.

208 We found that no precipitation product performed better in all models and each product performed
209 differently depending on the basin. This implies that the optimum dataset to use depends on the location
210 of the model. JRA-55 was very poor at capturing extreme rainfall and subsequently hydrograph peak
211 and inundation magnitude in almost all cases. This may be slightly influenced by the lower temporal
212 resolution, but it is unlikely that the small difference in observation frequency would result in such a
213 strong negative effect on model performance. ERA-5 consistently performed better than other reanalysis
214 datasets in terms of capturing the observed hydrograph peak. ERA-5, CFSR and MERRA2 were more
215 evenly matched in terms of floodplain water depth, inundation extent, and impacts. We find no cause to
216 favour any of these three datasets and suggest that all three could be adopted in parallel by reanalysis-
217 based flood models to capture the range of uncertainty.

218 Links between hydrograph performance and estimated numbers of inundated buildings are present but
219 the relationship is not consistent. For example, in the Tyne basin, CFSR estimates a higher gauge peak
220 than JRA-55 but, at the same time, inundates fewer buildings. Meanwhile, MERRA-2 only has the
221 lowest hydrograph peak in the Tyne, where it estimates the lowest total building inundation compared
222 to other models. CEH-GEAR1hr is also both generally higher in terms of both building inundation
223 and hydrograph peak, but the occasions where this is not the case do not correspond to the same basin.
224 These findings demonstrate that there is generally a positive relationship between peak hydrograph depth
225 and numbers of inundated buildings, but increased river depth does not always lead to greater inundation.
226 Therefore, hydrograph performance is not an entirely reliable metric for assessing the accuracy of flood
227 risk estimated using global reanalysis products.

228 The underestimation of inundation magnitude caused by using global precipitation data is counter to
229 the overestimation that results from using global DEM data, as demonstrated by McClean et al. (2020).
230 The negative inundation bias caused by using reanalysis precipitation is, however, not as strong as the
231 positive bias from global DEM products. This is because changes in rainfall input have a less significant
232 impact on the spatial distribution of flooding than changes in DEM input. Therefore, it is anticipated
233 that the combined effects of using both global DEM and global reanalysis precipitation would not cancel
234 themselves out and likely to produce a net positive bias.

235 Undoubtedly the effects shown here are specific to the study area and other locations may present different
236 patterns. Each reanalysis product may behave differently across climatic regions, for example. Areas
237 with highly constrained topography are unlikely to be strongly affected by the choice of precipitation
238 data, in terms of flood extent and numbers of inundated assets. This is because increases in total rainfall
239 volume will not greatly alter flood extent if there are no new available flow pathways. A key limitation to
240 applying our methodology in new locations is the requirement for high-quality gauge-based precipitation
241 datasets and river flow observations to compare against. Despite the caveat of locality, our results do
242 demonstrate the potential for underestimation of flood risk when reanalysis products are involved. This



243 underestimation has been replicated by previous studies in other areas (Sampson et al., 2014) and users
244 of models based on reanalysis data should be aware of this effect.

245 Conclusions

246 Using precipitation from global reanalysis datasets results in an underestimation of flood risk by 14-18 %
247 of inundated buildings and 29-44 % of median floodplain depth (Table 3, excluding JRA-55). The effect
248 is location-specific, though, and this study found that no product performed best across all five of the
249 catchments we studied. In some areas, the reanalysis data did result in similar levels of inundation to
250 the national observed precipitation product (CEH-GEAR1hr). This is a positive message for the use of
251 reanalysis data in flood risk modelling generally and future progress in forecast models will undoubtedly
252 reduce this gap even further.

253 As climatic and land-use changes increase flood hazard, the importance of accurately understanding
254 current and future flood risk is increasing. Reanalysis data has enabled flood risk assessments to be
255 undertaken more widely. However, this analysis shows global or regional reanalysis data should not be
256 considered as a replacement for local, high resolution, observations. Uncertainties in flood risk assessment
257 using reanalysis data need to be properly quantified and communicated to insurers, local and national
258 authorities and communities, to ensure flood risk management decisions are not misinformed.

259 While reanalysis datasets do show promising and improving results (ERA-5 achieved a mean absolute
260 hydrograph peak error of 29.4 %, equivalent to CEH-GEAR1hr and CFSR only inundated on average
261 14.4 % fewer buildings than CEH-GEAR1hr), caution should be used when interpreting outputs from any
262 models based on them. We suggest that multiple products, such as ERA-5, CFSR and MERRA-2, should
263 be used where possible to capture the full range of uncertainty. This is because each of these products
264 has been shown to perform better in different areas or when using different performance measures. Based
265 on the comparatively strong negative bias in inundation and flood peak shown here, JRA-55 should not
266 be used in flood risk modelling. However, as highlighted, certain products may perform better in other
267 areas and further research is needed to assess new and existing reanalysis products for flood modelling
268 across a wider range of climatic regions. To enable this, a more systematic international strategy for the
269 collection of rainfall data is needed to ensure more complete global coverage of validation data, building
270 on efforts from Lewis et al. (2019).

271 Code/Data availability

272 The reanalysis products can be downloaded using the DOIs in Table 1. All model results and code used
273 to generate figures will be made available by final submission.

274 Author contribution

275 FM processed the data and executed the simulations. FM prepared the manuscript with contributions
276 from all co-authors.

277 Competing interests

278 The authors declare that they have no conflict of interest.

279 Acknowledgements

280 The authors were supported by the Natural Environmental Research Council (NERC) Centre for Doctoral
281 Training for Data, Risk and Environmental Analytical Methods (DREAM), TWENTY 65: Tailored



282 Water Solutions for Positive Impact and Willis Research Network. The City Catchment Analysis Tool
283 (CityCAT) was developed and provided by Vassilis Glenis. Chris Kilsby acknowledges the support of
284 the Willis Research Network.

285 References

- 286 Albergel, C., Dutra, E., Munier, S., Calvet, J.-C., Munoz-Sabater, J., de Rosnay, P., & Balsamo, G. (2018,
287 jun). ERA-5 and ERA-Interim driven ISBA land surface model simulations: which one performs
288 better? *Hydrology and Earth System Sciences*, *22*(6), 3515–3532. Retrieved from [https://](https://doi.org/10.5194/2Fhess-22-3515-2018)
289 doi.org/10.5194/2Fhess-22-3515-2018 doi: 10.5194/hess-22-3515-2018
- 290 Alfieri, L., Burek, P., Dutra, E., Krzeminski, B., Muraro, D., Thielen, J., & Pappenberger, F. (2013,
291 mar). GloFAS – global ensemble streamflow forecasting and flood early warning. *Hydrology and*
292 *Earth System Sciences*, *17*(3), 1161–1175. Retrieved from [https://doi.org/10.5194/2Fhess-17-](https://doi.org/10.5194/2Fhess-17-1161-2013)
293 [1161-2013](https://doi.org/10.5194/2Fhess-17-1161-2013) doi: 10.5194/hess-17-1161-2013
- 294 Andreadis, K. M., Schumann, G. J.-P., Stampoulis, D., Bates, P. D., Brakenridge, G. R., & Kettner,
295 A. J. (2017, oct). Can Atmospheric Reanalysis Data Sets Be Used to Reproduce Flooding Over
296 Large Scales? *Geophysical Research Letters*, *44*(20), 10,369–10,377. Retrieved from [https://](https://doi.org/10.1002/2F2017gl075502)
297 doi.org/10.1002/2F2017gl075502 doi: 10.1002/2017gl075502
- 298 Beck, H. E., Vergopolan, N., Pan, M., Levizzani, V., van Dijk, A. I. J. M., Weedon, G. P., ... Wood,
299 E. F. (2017, dec). Global-scale evaluation of 22 precipitation datasets using gauge observations
300 and hydrological modeling. *Hydrology and Earth System Sciences*, *21*(12), 6201–6217. Retrieved
301 from <https://doi.org/10.5194/2Fhess-21-6201-2017> doi: 10.5194/hess-21-6201-2017
- 302 Chawla, I., & Mujumdar, P. (2020, sep). Evaluating rainfall datasets to reconstruct floods in data-
303 sparse Himalayan region. *Journal of Hydrology*, *588*, 125090. Retrieved from [https://doi.org/](https://doi.org/10.1016/2Fj.jhydrol.2020.125090)
304 [10.1016/2Fj.jhydrol.2020.125090](https://doi.org/10.1016/2Fj.jhydrol.2020.125090) doi: 10.1016/j.jhydrol.2020.125090
- 305 Chow, V. T. (1959). *Open-channel hydraulics* (Vol. 1). McGraw-Hill New York.
- 306 Dee, D. P., Uppala, S. M., Simmons, A. J., Berrisford, P., Poli, P., Kobayashi, S., ... Vitart, F.
307 (2011). The ERA-Interim reanalysis: configuration and performance of the data assimilation
308 system. *Quarterly Journal of the Royal Meteorological Society*, *137*(656), 553–597. doi: 10.1002/
309 qj.828
- 310 ECMWF. (2018). *ERA5 hourly data on single levels from 1979 to present*. Copernicus Climate Change
311 Service. doi: <https://doi.org/10.24381/cds.adbb2d47>
- 312 Environment Agency. (2019). *What is the risk of flooding from surface water map*. Retrieved
313 from [https://assets.publishing.service.gov.uk/government/uploads/system/uploads/](https://assets.publishing.service.gov.uk/government/uploads/system/uploads/attachment_data/file/842485/What-is-the-Risk-of-Flooding-from-Surface-Water-Map.pdf)
314 [attachment_data/file/842485/What-is-the-Risk-of-Flooding-from-Surface-Water-Map](https://assets.publishing.service.gov.uk/government/uploads/system/uploads/attachment_data/file/842485/What-is-the-Risk-of-Flooding-from-Surface-Water-Map.pdf)
315 [.pdf](https://assets.publishing.service.gov.uk/government/uploads/system/uploads/attachment_data/file/842485/What-is-the-Risk-of-Flooding-from-Surface-Water-Map.pdf)
- 316 Gelaro, R., McCarty, W., Suárez, M. J., Todling, R., Molod, A., Takacs, L., ... Zhao, B. (2017, jul). The
317 Modern-Era Retrospective Analysis for Research and Applications Version 2 (MERRA-2). *Journal*
318 *of Climate*, *30*(14), 5419–5454. Retrieved from <https://doi.org/10.1175/2Fjcli-d-16-0758.1>
319 doi: 10.1175/jcli-d-16-0758.1
- 320 Glenis, V., Kutija, V., & Kilsby, C. (2018, nov). A fully hydrodynamic urban flood modelling system
321 representing buildings green space and interventions. *Environmental Modelling & Software*, *109*,
322 272–292. Retrieved from <https://doi.org/10.1016/2Fj.envsoft.2018.07.018> doi: 10.1016/
323 j.envsoft.2018.07.018
- 324 Global Modeling and Assimilation Office. (2015). *MERRA-2 tavg1_2d_flux_Nx: 2d,1-Hourly,Time-*
325 *Averaged,Single-Level,Assimilation,Surface Flux Diagnostics V5.12.4*. Greenbelt, MD, USA, God-
326 dard Earth Sciences Data and Information Services Center. Retrieved from [https://doi.org/](https://doi.org/10.5067/7MCPBJ41Y0K6)
327 [10.5067/7MCPBJ41Y0K6](https://doi.org/10.5067/7MCPBJ41Y0K6) doi: <https://doi.org/10.5067/7MCPBJ41Y0K6>
- 328 Harrigan, S., Zsoter, E., Alfieri, L., Prudhomme, C., Salamon, P., Wetterhall, F., ... Pappenberger, F.
329 (2020, jan). GloFAS-ERA5 operational global river discharge reanalysis 1979–present. Retrieved
330 from <https://doi.org/10.5194/2Fessd-2019-232> doi: 10.5194/essd-2019-232
- 331 Hirpa, F. A., Salamon, P., Alfieri, L., del Pozo, J. T., Zsoter, E., & Pappenberger, F. (2016, apr).
332 The Effect of Reference Climatology on Global Flood Forecasting. *Journal of Hydrometeorology*,
333 *17*(4), 1131–1145. Retrieved from <https://doi.org/10.1175/2Fjhm-d-15-0044.1> doi: 10.1175/
334 jhm-d-15-0044.1



- 335 Hua, W., Zhou, L., Nicholson, S. E., Chen, H., & Qin, M. (2019, aug). Correction to: Assessing reanalysis data for understanding rainfall climatology and variability over Central Equatorial Africa. *Climate Dynamics*, *53*(7-8), 5139–5139. Retrieved from <https://doi.org/10.1007/s00382-019-04918-7> doi: 10.1007/s00382-019-04918-7
- 336
337
338
- 339 Japan Meteorological Agency. (2013). *JRA-55: Japanese 55-year Reanalysis, Daily 3-Hourly and 6-Hourly Data*. Boulder CO: Research Data Archive at the National Center for Atmospheric Research, Computational and Information Systems Laboratory. doi: 10.5065/D6HH6H41
- 340
341
- 342 Kalnay, E., Kanamitsu, M., Kistler, R., Collins, W., Deaven, D., Gandin, L., ... Joseph, D. (1996, mar). The NCEP/NCAR 40-Year Reanalysis Project. *Bulletin of the American Meteorological Society*, *77*(3), 437–471. Retrieved from <https://doi.org/10.1175/2F1520-0477%281996%29077%3C0437%3Atnyrp%3E2.0.co%3B2> doi: 10.1175/1520-0477(1996)077<0437:tnyrp>2.0.co;2
- 343
344
345
- 346 Kobayashi, S., Ota, Y., Harada, Y., Ebata, A., Moriya, M., Onoda, H., ... Takahashi, K. (2015). The JRA-55 Reanalysis: General Specifications and Basic Characteristics. *Journal of the Meteorological Society of Japan. Ser. II*, *93*(1), 5–48. Retrieved from <https://doi.org/10.2151/jmsj.2015-001> doi: 10.2151/jmsj.2015-001
- 347
348
349
- 350 Lehner, B., & Grill, G. (2014). *HydroBASINS: Global watershed boundaries and sub-basin delineations derived from HydroSHEDS data at 15 second resolution—Technical documentation version 1. c* (Vol. 27; Tech. Rep. No. 2013). Retrieved from <https://www.hydrosheds.org/images/inpages/HydroBASINS{ }TechDoc{ }v1c.pdf>
- 351
352
353
- 354 Lewis, E., Fowler, H., Alexander, L., Dunn, R., McClean, F., Barbero, R., ... Blenkinsop, S. (2019, jul). GSDR: A Global Sub-Daily Rainfall Dataset. *Journal of Climate*, *32*(15), 4715–4729. Retrieved from <https://doi.org/10.1175/2Fjcli-d-18-0143.1> doi: 10.1175/jcli-d-18-0143.1
- 355
356
- 357 Lewis, E., Quinn, N., Blenkinsop, S., Fowler, H. J., Freer, J., Tanguy, M., ... Woods, R. (2018, sep). A rule based quality control method for hourly rainfall data and a 1km resolution gridded hourly rainfall dataset for Great Britain: CEH-GEAR1hr. *Journal of Hydrology*, *564*, 930–943. Retrieved from <https://doi.org/10.1016%2Fj.jhydrol.2018.07.034> doi: 10.1016/j.jhydrol.2018.07.034
- 358
359
360
- 361 Mahto, S. S., & Mishra, V. (2019, aug). Does ERA-5 Outperform Other Reanalysis Products for Hydrologic Applications in India? *Journal of Geophysical Research: Atmospheres*, *124*(16), 9423–9441. Retrieved from <https://onlinelibrary.wiley.com/doi/10.1029/2019JD031155> doi: 10.1029/2019JD031155
- 362
363
364
- 365 McClean, F., Dawson, R., & Kilsby, C. (2020, oct). Implications of Using Global Digital Elevation Models for Flood Risk Analysis in Cities. *Water Resources Research*, *56*(10). Retrieved from <https://doi.org/10.1029/2F2020wr028241> doi: 10.1029/2020wr028241
- 366
367
- 368 Ordnance Survey. (2017). *OS Terrain 50 User Guide v1.3* (Tech. Rep.). Retrieved from <https://www.ordnancesurvey.co.uk/documents/os-terrain-50-user-guide.pdf>
- 369
- 370 Ordnance Survey. (2020). OS VectorMap local technical specification. Retrieved from <https://www.ordnancesurvey.co.uk/documents/os-vectormap-local-technical-specification.pdf> accessedon={MondayApril132020} accessedon={MondayApril132020}
- 371
372
- 373 Pappenberger, F., Dutra, E., Wetterhall, F., & Cloke, H. L. (2012, nov). Deriving global flood hazard maps of fluvial floods through a physical model cascade. *Hydrology and Earth System Sciences*, *16*(11), 4143–4156. Retrieved from <https://doi.org/10.5194/2Fhess-16-4143-2012> doi: 10.5194/hess-16-4143-2012
- 374
375
376
- 377 Reichle, R. H., Liu, Q., Koster, R. D., Draper, C. S., Mahanama, S. P. P., & Partyka, G. S. (2017, feb). Land Surface Precipitation in MERRA-2. *Journal of Climate*, *30*(5), 1643–1664. Retrieved from <https://doi.org/10.1175/2Fjcli-d-16-0570.1> doi: 10.1175/jcli-d-16-0570.1
- 378
379
- 380 Rienecker, M. M., Suarez, M. J., Gelaro, R., Todling, R., Bacmeister, J., Liu, E., ... Woollen, J. (2011, jul). MERRA: NASA's Modern-Era Retrospective Analysis for Research and Applications. *Journal of Climate*, *24*(14), 3624–3648. Retrieved from <https://doi.org/10.1175/2Fjcli-d-11-00015.1> doi: 10.1175/jcli-d-11-00015.1
- 381
382
383
- 384 Saha, S., Moorthi, S., Pan, H.-L., Wu, X., Wang, J., Nadiga, S., ... Goldberg, M. (2010, aug). The NCEP Climate Forecast System Reanalysis. *Bulletin of the American Meteorological Society*, *91*(8), 1015–1058. Retrieved from <https://doi.org/10.1175/2F2010bams3001.1> doi: 10.1175/2010bams3001.1
- 385
386
387
- 388 Saha, S., Moorthi, S., Pan, H.-L., Wu, X., Wang, J., Nadiga, S., ... Goldberg, M. (2010). *NCEP Climate Forecast System Reanalysis (CFSR) Selected Hourly Time-Series Products, January 1979 to December 2010*. Boulder CO: Research Data Archive at the National Center for Atmospheric
- 389
390



- 391 Research, Computational and Information Systems Laboratory. Retrieved from [https://doi.org/](https://doi.org/10.5065/D6513W89)
392 10.5065/D6513W89
- 393 Sampson, C. C., Fewtrell, T. J., O'Loughlin, F., Pappenberger, F., Bates, P. B., Freer, J. E., & Cloke,
394 H. L. (2014, jun). The impact of uncertain precipitation data on insurance loss estimates using a
395 flood catastrophe model. *Hydrology and Earth System Sciences*, 18(6), 2305–2324. Retrieved from
396 <https://doi.org/10.5194%2Fhess-18-2305-2014> doi: 10.5194/hess-18-2305-2014
- 397 Schumann, G. J.-P., Neal, J. C., Voisin, N., Andreadis, K. M., Pappenberger, F., Phanthuwongpakdee,
398 N., ... Bates, P. D. (2013, oct). A first large-scale flood inundation forecasting model. *Water Re-*
399 *sources Research*, 49(10), 6248–6257. Retrieved from <https://doi.org/10.1002%2Fwrcr.20521>
400 doi: 10.1002/wrcr.20521
- 401 Seyyedi, H., Anagnostou, E. N., Beighley, E., & McCollum, J. (2015, oct). Hydrologic evaluation of
402 satellite and reanalysis precipitation datasets over a mid-latitude basin. *Atmospheric Research*,
403 164–165, 37–48. Retrieved from <https://doi.org/10.1016%2Fj.atmosres.2015.03.019> doi:
404 10.1016/j.atmosres.2015.03.019
- 405 Suzuki, T., Yamazaki, D., Tsujino, H., Komuro, Y., Nakano, H., & Urakawa, S. (2017, dec). A dataset of
406 continental river discharge based on JRA-55 for use in a global ocean circulation model. *Journal of*
407 *Oceanography*, 74(4), 421–429. Retrieved from [https://doi.org/10.1007%2Fs10872-017-0458](https://doi.org/10.1007%2Fs10872-017-0458-5)
408 -5 doi: 10.1007/s10872-017-0458-5
- 409 Tanguy, H.-I. D. V., M.; Dixon. (2019). Gridded estimates of daily and monthly areal rainfall for the
410 United Kingdom (1890-2017) [CEH-GEAR].
411 doi: 10.5285/ce9ab43d-a4fe-4e73-afd5-cd4fc4c82556
- 412 Towner, J., Cloke, H. L., Zsoter, E., Flamig, Z., Hoch, J. M., Bazo, J., ... Stephens, E. M. (2019,
413 jul). Assessing the performance of global hydrological models for capturing peak river flows in
414 the Amazon basin. *Hydrology and Earth System Sciences*, 23(7), 3057–3080. Retrieved from
415 <https://doi.org/10.5194%2Fhess-23-3057-2019> doi: 10.5194/hess-23-3057-2019
- 416 Winsemius, H. C., Beek, L. P. H. V., Jongman, B., Ward, P. J., & Bouwman, A. (2013, may). A
417 framework for global river flood risk assessments. *Hydrology and Earth System Sciences*, 17(5),
418 1871–1892. Retrieved from <https://doi.org/10.5194%2Fhess-17-1871-2013> doi: 10.5194/
419 hess-17-1871-2013
- 420 Xu, H., Xu, C.-Y., Chen, S., & Chen, H. (2016, nov). Similarity and difference of global reanalysis
421 datasets (WFD and APHRODITE) in driving lumped and distributed hydrological models in a
422 humid region of China. *Journal of Hydrology*, 542, 343–356. Retrieved from [https://doi.org/](https://doi.org/10.1016%2Fj.jhydrol.2016.09.011)
423 10.1016/j.jhydrol.2016.09.011 doi: 10.1016/j.jhydrol.2016.09.011
- 424 Zhu, Q., Xuan, W., Liu, L., & Xu, Y.-P. (2016, apr). Evaluation and hydrological application of
425 precipitation estimates derived from PERSIANN-CDR TRMM 3B42V7 and NCEP-CFSR over
426 humid regions in China. *Hydrological Processes*, 30(17), 3061–3083. Retrieved from [https://](https://doi.org/10.1002%2Fhyp.10846)
427 doi: 10.1002/hyp.10846 doi: 10.1002/hyp.10846